Heliyon 10 (2024) e33580

Contents lists available at ScienceDirect

Heliyon

journal homepage: www.cell.com/heliyon

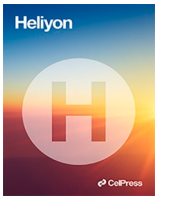

Research article

Synthesis of $La_{1-x}Sr_xCoO_{3-\delta}$ and its catalytic oxidation of NO and its reaction path

Yige Guo [a,*], Xiaoxue Niu [b], Huaiyu Yang [c], Liwen Chen [a], Yizhen Ren [a], Huining Guo [b], Bo Wu [d,**]

[a] College of Geology and Environment, Xian University of Science and Technology, Xian, 710054, China
[b] School of Environment, Renmin University of China, Beijing, 100872, China
[c] School of Environmental Engineering, Loughborough University, Loughborough, LE11 3RP, UK
[d] Henan International Joint Laboratory of Environment and Resources, School of Ecology and Environment, Engineering Research Center of Advanced Functional Material Manufacturing of Ministry of Education, School of Chemical Engineering, Zhengzhou University, 450001, China

ARTICLE INFO

Keywords:
NO oxidation
Perovskite
$La_{1-x}Sr_xCoO_{3-\delta}$
Catalyst

ABSTRACT

The oxidation rate of NO to NO_2 is a critical parameter in the removal of NO_x within selective catalytic reduction (SCR) systems. $LaCoO_{3-\delta}$ is a kind of potential catalyst to enhance the oxidation of NO to NO_2, it may offers an economic and stable alternative to noble metal catalysts, particularly at elevated temperatures. This study aimed to enhance the catalytic efficiency of $LaCoO_{3-\delta}$ through strontium (Sr) doping. $La_{1-x}Sr_xCoO_{3-\delta}$ (with varying x values of 0.1, 0.2, 0.3, 0.4) was synthesized using a sol-gel method. $La_{1-x}Sr_xCoO_{3-\delta}$ exhibited superior NO oxidation catalytic activity compared to $LaCoO_{3-\delta}$, with the most notable enhancement observed at $x = 0.3$ (84 % conversion). This improvement can be attributed to the substitution of La^{3+} with Sr^{2+}, which induces lattice distortion and charge imbalance, thereby creating more oxygen vacancies that enhance the catalytic oxidation capability of $La_{1-x}Sr_xCoO_{3-\delta}$. However, it's important to note that an excessive amount of Sr can result in the formation of $SrCO_3$ deposits on the surface of $La_{1-x}Sr_xCoO_{3-\delta}$, thereby diminishing its catalytic oxidation performance. The catalytic oxidation reaction behavior adhered most closely to the O_2-adsorbed E-R model, the surface defects in $La_{1-x}Sr_xCoO_{3-\delta}$ playing a pivotal role in the catalytic reaction.

1. Introduction

Diesel vehicles have gained widespread popularity due to their economic advantages and low carbon dioxide emissions [1]. However, it's important to acknowledge that diesel engines make a significant contribution to nitrogen oxide (NOx) pollution. In China, diesel vehicles are responsible for approximately 88 % of the total NOx emissions from mobile sources. NOx, as a typical pollutant, poses a serious threat to environmental health and public safety [2]. Selective catalytic reduction (SCR) stands as an efficient technology for mitigating NO_x emissions [3]. An effective strategy to enhance the SCR process is to increase the NO_2 to NO ratio in the reaction system to a 1:1 level. This adjustment stimulates a rapid reaction and results in a five-fold increase in the reaction rate [4,5]. However, the concentration of NO in diesel exhaust is relatively low, making it challenging to achieve rapid oxidation of NO to NO_2

* Corresponding author.
** Corresponding author.
E-mail addresses: guoyige999@163.com (Y. Guo), wb@zzu.edu.cn (B. Wu).

https://doi.org/10.1016/j.heliyon.2024.e33580
Received 18 March 2024; Received in revised form 5 May 2024; Accepted 24 June 2024
Available online 3 July 2024

without the use of a catalyst [6]. Commonly employed catalysts for this NO-to-NO_2 oxidation process include noble metals (such as Pt, Pd, Ru), metal oxides (like CeO_2 and ZrO_2), and perovskite materials such as $LaMnO_3$ and $LaCoO_{3-\delta}$. However, noble metal catalysts are associated with issues such as high-temperature sintering, susceptibility to deactivation, and high economic costs [7,8].

In recent years, there has been significant research on perovskite catalysts due to their straightforward production process, cost-effectiveness, and structural flexibility [9–11]. Perovskite materials, with a general formula of ABO_3, have proven to be an economically viable alternative to noble metal catalysts in oxidation processes. When elements are substituted on either the A- or B-sites of the perovskite structure, they transform into $(AxA'1-x)(ByB'1-y)O_3$ compositions, leading to the generation of additional oxygen vacancies [12,13]. These vacancies play a crucial role in improving the catalytic oxidation performance of perovskite materials [14]. The key to enhancing catalytic oxidation performance lies in the modification of perovskite and the adjustment of its lattice defects to generate more oxygen vacancies. Libby et al. demonstrated the potential of using perovskite-type composite oxides as catalysts instead of precious metal catalysts to treat automobile exhaust gas [15]. It has been demonstrated that perovskites exhibit improved catalytic oxidation performance when cobalt (Co) is present at the B-site. Remeika et al. [16] found that manganese oxides and cobalt oxides have extremely high catalytic oxidation activity. Ma et al. [2] also studied the NO oxidation properties of Co_3O_4 nanorods and nanoparticles, which were mainly exposed to the catalytically active lattice surface of (110). Co_3O_4 nanorods can expose more active sites and have better NO conversion rate. Wu et al. [17] introduced the effect of B-site partial substitution on $LaMn_{0.25}Co_{0.75}O_3$ (M = Cu, Mn, Fe), and found that ion substitution would not destroy the perovskite structure of $LaCoO_3$, but also improve its catalytic performance. This is attributed to the improved reduction performance of the catalyst and the increased content of oxygen defect sites in the catalyst. The partial substitution of copper significantly reduces the effect of NO preferential adsorption on the $LaCoO_3$ catalyst on the adsorption of CO, promotes the adsorption and activation of O_2 by perovskite, and produces more active oxygen species on the catalyst surface. Vazhayil et al. [18] doped Co into the B site of $LaMnO_3$, and the samples doped with Co still maintained a rhomboidal crystal structure. The presence of Co made the B-site cations in a higher oxidation state, which significantly improved the OER activity and stability of $LaMnO_3$. Therefore, in this study, a series of $La_{1-x}Sr_xCoO_{3-\delta}$ materials were synthesized through strontium (Sr) doping using a sol-gel method. The catalytic capabilities of these $La_{1-x}Sr_xCoO_{3-\delta}$ compounds for NO-to-NO_2 oxidation were investigated under varying levels of Sr doping and different reaction conditions.

2. Materials and methods

2.1. Materials

$La(NO_3)_3{\cdot}6H_2O$ (AR), $Co(NO_3)_3{\cdot}6H_2O$ (AR), $Sr(NO_3)_2$ (AR), $C_6H_8O_7{\cdot}H_2O$ (AR), and HCl (99 wt%) were purchased from Beijing Tongguang Chemical Company. PEO-PPO-PEO (AR) was provided by Sinopharm Chemical Reagent Co., Ltd (China), and $C_8H_2O_4Si$ (AR) was sourced from Shanghai Aladdin Biochemical Technology Co., Ltd. O_2/He (20.00 %), N_2 (99.999 %), He (99.999 %), and NO/N_2 (3.02 % NO) were obtained from Beijing Hepu Gas Industry Co., Ltd. Deionized water was used throughout the experiments, and none of the reagents underwent double purification before their use.

2.2. Preparation of $La_{1-x}Sr_xCoO_{3-\delta}$

$La_{1-x}Sr_xCoO_{3-\delta}$ (with x = 0, 0.1, 0.2, 0.3, 0.4) were synthesized via the Sol-gel method [19]. The specific preparation process was carried out as follows. $La(NO_3)_3{\cdot}6H_2O$, $Co(NO_3)_3{\cdot}6H_2O$, and $Sr(NO_3)_2$ were dissolved in deionized water at predetermined ratios. Citric acid was employed as a chelating agent and added to the solution, maintaining a mole ratio of 1:1 between citric acid and the total metal ions. The solution was stirred at 80 °C until a gel was formed. Subsequently, the gel was dried at 90 °C for 12 h to yield a dried gel. Then, the dried gel was finely ground and subjected to calcination in a muffle furnace at 700 °C for 5 h to promote the formation of the perovskite structure, with a heating rate of 10 °C·min^{-1}.

2.3. Characterization of adsorbents

The crystal structure of $La_{1-x}Sr_xCoO_{3-\delta}$ was analyzed using X-ray diffraction (XRD) with a Rigaku D/max 2500X instrument. Additionally, the functional groups, surface chemical composition, and ion valence states of the samples were characterized through X-ray photoelectron spectroscopy (XPS) with an ESCALAB 250 Xi instrument and Fourier-transform infrared spectroscopy (FT-IR) using a Nicolet 6700 spectrometer.

2.4. Catalyst activity testing

To further assess the obtained samples, various techniques were employed. Hydrogen temperature-programmed reduction (H_2-TPR), oxygen temperature-programmed desorption (O_2-TPD), and nitrogen oxide temperature-programmed desorption (NO-TPD) were utilized for the comprehensive characterization of the samples. These methods provide valuable insights into the chemical and structural properties of the $La_{1-x}Sr_xCoO_{3-\delta}$ materials, offering a thorough analysis of their behavior and reactivity.

The assessment of NO oxidation activity was conducted in a fixed-bed quartz micro-reactor, operating under steady-flow conditions. In each test, 0.1 g of catalysts, sieved to 40–60 mesh, was employed. The reactant gas composition typically consisted of 500 ppm NO, 5 % O_2, and the balance N_2. The total flow rate was set at 200 mL min^{-1}, resulting in a Gas Hourly Space Velocity (GHSV) of 120,000 h^{-1}. Data recording was initiated once the oxidation reaction reached a steady state, which typically occurred after 10 min at

each measuring temperature.

To monitor the concentrations of reactants and products in real-time, an online Fourier-transform infrared (FT-IR) spectrometer, specifically the Nicolet Antaris IGS Gas Analyzer, was utilized. NO conversion was calculated using the following equation:

$$C_{NO}(\%) = \frac{NO_{in} - NO_{out}}{NO_{out}} \times 100\% \quad (1)$$

where $C_{NO}(\%)$ represents the conversion efficiency of NO, NO_{in} is defined as the NO concentration of the gas inlet for the reactor, and NO_{out} is the NO volumetric concentration at the outlet of the reactor.

3. Results and discussion

3.1. Characterization of $La_{1-x}Sr_xCoO_{3-\delta}$

The X-ray diffraction (XRD) patterns of the synthesized $La_{1-x}Sr_xCoO_{3-\delta}$ materials are shown in Fig. 1. Eleven distinctive characteristic peaks corresponding to $LaCoO_{3-\delta}$, as per the standard card (PDF#84–0848) [20], were observed at specific 2θ values: 23.2, 32.9, 33.3, 40.7, 47.5, 58.9, 59.8, 68.9, 69.9, 78.8, and 79.5. The presence of doublet peaks at 2θ values of 32.89° and 33.27° suggests the formation of a rhombohedral crystal structure [21].

As the Sr^{2+} concentration increased in the perovskite unit cells, a systematic shift in the diffraction angles towards lower values was observed. This phenomenon can be attributed to the expansion of the perovskite unit cell resulting from the substitution of smaller La^{3+} cations (r = 0.136 nm) with larger Sr^{2+} cations (r = 0.144 nm). At lower strontium substitution levels (x < 0.30), the perovskite structure maintained its rhombohedral symmetry, with a doublet peak in the 2θ range of 33–34°.

However, with an increase in strontium substitution (i.e., x = 0.80), the rhombohedral structure weakened, and the doublet peak gradually merged into a singlet peak. This shift in crystal symmetry signified the transition from a rhombohedral structure to a cubic structure with higher strontium substitution (x = 0.4) [22,23]. For $LaCoO_{3-\delta}$, the substitution of Sr^{2+} for La^{3+} is constrained, as reported in previous studies [24]. With the introduction of Sr doping, new diffraction peaks characteristic of $SrCO_3$ start to emerge in the XRD patterns, notably at 2θ values of 25.8°, 29.3°, 30.1°, 36.8°, 44.1°, and 50.0°. These peaks become sharper with increased Sr doping, indicating the presence of phase segregation within the material [25]. This phenomenon suggests that beyond a certain threshold of Sr doping, the crystalline structure undergoes significant changes.

Fig. 2 shows the FT-IR spectra of $La_{1-x}Sr_xCoO_{3-\delta}$. In these spectra, distinct vibrational modes associated with the crystal structure are evident. Specifically, the O–Co–O bending and O–Co stretching vibrations of octahedrally coordinated CoO_6 units are discernible at 418 cm^{-1} and 674 cm^{-1}, respectively. Additionally, vibrations related to La–*O*–Co bending are observed at 694 cm^{-1} [26], indicating the presence of La in the compound. Notably, as the Sr concentration increases, a new peak emerges in the FT-IR spectrum, approximately at 852 cm^{-1}. This particular peak is attributed to Sr–O vibrations [27,28]. The blue shift observed in the peak position at 594 cm^{-1}, along with the weakening of peak intensity, can be attributed to the partial substitution of Sr for La and the concurrent presence of Sr–*O*–Co and La–*O*–Co bonds. Additionally, it is notable that the force constant (k) of the La–*O*–Co bond gradually decreases with the increasing Sr doping, leading to an increase in surface lattice distortion and an extension of the Co–O distance. The substitution of Sr^{2+} for La^{3+} in the perovskite lattice weakens the La–*O*–Co bond vibrations, making the reduction of Co^{3+} easier, and contributing to enhancing the catalytic activity of the oxidation reaction [17]. This structural modification is advantageous for the adsorption of NO and the enhancement of oxygen activation [20,29]. These findings align with the results obtained from XRD analysis,

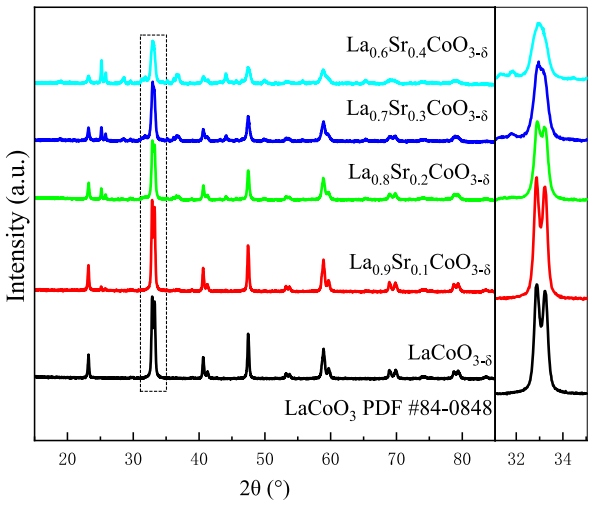

Fig. 1. XRD patterns of $La_{1-x}Sr_xCoO_{3-\delta}$ (x = 0,0.1,0.2,0.3,0.4).

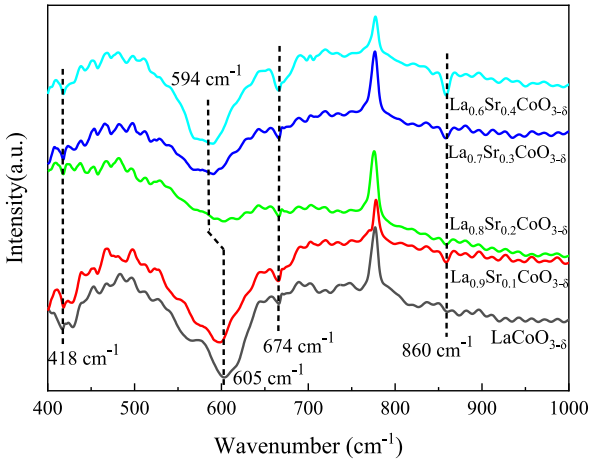

Fig. 2. FT-IR patterns of $La_{1-x}Sr_xCoO_{3-\delta}$(x = 0,0.1,0.2,0.3,0.4).

providing further support for the structural changes of $LaCoO_{3-\delta}$ induced by Sr doping and their implications for catalytic properties.

The catalytic efficiency is closely associated with the reduction capacity of oxygen adsorbed on the catalyst's surface. A notable enhancement in the catalytic efficiency is anticipated due to the significant reducing ability of the adsorbed oxygen in the NO and Oads reaction. This increased reducing capacity subsequently leads to an improvement of the NO oxidation activity. Consequently, the reducibility of the catalysts plays a pivotal role in influencing the NO oxidation activity, and this reducibility is assessed through H_2-TPR tests. It is important to note that, as La^{3+} is non-reducible [30], the observed reduction peaks can be attributed solely to the reduction of Co species.

The H_2-TPR profiles for $La_{1-x}Sr_xCoO_{3-\delta}$ are shown in Fig. 3 [31]. In these profiles, two distinct reduction regions are evident, spanning the temperature ranges of 200–400 °C and 400–600 °C for all catalysts. Within the first reduction stage, two successive peaks are observed. The initial peak is attributed to the reduction of Co^{3+} to Co^{2+}, while the subsequent peak corresponds to the formation of a millerite structure ($LaCoO_{2.5}$) [32]. The larger peak in the second reduction stage signifies the reduction of Co^{2+} to Co0 [33]. Compared to the $LaCoO_{3-\delta}$ catalyst, the first two reduction peaks of $La_{1-x}Sr_xCoO_{3-\delta}$ exhibit a slight shift towards lower temperatures. Simultaneously, the areas under these reduction peaks in the lower-temperature range increase. Due to weakness of the La–*O*–Co bond vibrations in the perovskite lattice, as shown in the analysis of FT-IR, Co^{3+} is easier to reduce, which helps to improve the catalytic activity of the oxidation reaction [17]. Additionally, the fact that $La_{1-x}Sr_xCoO_{3-\delta}$ exhibits lower reduction temperatures may also be attributed to its higher lattice oxygen activity and mobility [34]. This could be attributed to the increased generation of oxygen vacancies due to Sr doping [35] which is consistent with the FT-IR results. These oxygen vacancies facilitate oxygen adsorption and the migration of lattice oxygen, thus making the oxidation of H_2 more accessible and reducing its reduction temperature. This is supported by the gradual shift of high-temperature reduction peaks towards lower temperatures [36]. When the doping amount of Sr increases and x increases from 0 to 0.4 [36], the high-temperature reduction peak of H_2 moves to a lower temperature, indicating that oxygen vacancy promotes the activation of oxygen adsorption and lattice oxygen migration, thus reducing the reduction temperature of H_2 and improving the oxidation reaction of H_2. These results indicate that Sr doping with an appropriate substitution rate can improve the reducibility of $LaCoO_{3-\delta}$. Among these catalysts, the largest reduction peak area and relatively lower reduction peak temperature of

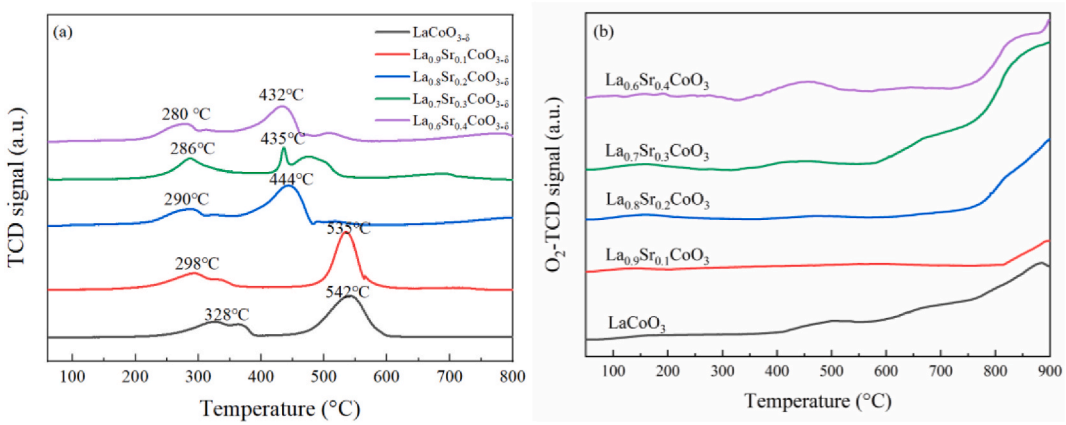

Fig. 3. H_2-TPR(a) and O_2-TPD(b) of $La_{1-x}Sr_xCO_{3-\delta}$(x = 0,0.1,0.2,0.3,0.4).

$La_{0.7}Sr_{0.3}CoO_{3-\delta}$ indicate exceptional oxidation capabilities.

Oxygen Temperature Programmed Desorption (O_2-TPD) experiments were conducted to characterize the oxygen mobility of $La_{1-x}Sr_xCoO_{3-\delta}$. Fig. 3b illustrates the oxygen desorption profiles, three distinct peaks were observed in the O_2-TPD profiles. The first peak is centered at 150 °C and exhibits very low intensity. This peak corresponds to the rapid re-oxidation of reduced cobalt species. Notably, $La_{0.7}Sr_{0.3}CoO_{3-\delta}$ displays the highest oxygen consumption at 150 °C, suggesting that cobalt (Co) is more readily re-oxidized [32]. The second peak, spanning the temperature range of 200–500 °C, is attributed to the removal of adsorbed oxygen species (referred to as OA). These oxygen species play a pivotal role in the catalytic oxidation of nitric oxide (NO) [37]. At higher temperatures, a desorption peak above 500 °C is observed, signifying the release of oxygen from the bulk (referred to as OL). This peak reflects the mobility of lattice oxygen within the perovskite structure [38].

The intensity of the O_A desorption peak in the Sr-doped samples is greater than that in $LaCoO_{3-\delta}$, and this observation is consistent with the conclusions drawn from X-ray Photoelectron Spectroscopy (XPS) analysis. Furthermore, the OA desorption peak in the Sr-doped samples is detected at lower temperature compared to $LaCoO_{3-\delta}$, indicating a higher reactivity of its chemically adsorbed oxygen species [39]. As previously observed in the H_2 Temperature Programmed Reduction (H_2–TPR) experiments, the introduction of Sr^{2+} by substituting La^{3+} leads to the creation of positive charge defects, which are balanced by the formation of oxygen vacancies. Notably, the substitution of La by Sr enhances the overall formation of OA, particularly when the lanthanum substitution degree reaches 0.3. These findings suggest that the enhanced intensity and lower temperature of the OA desorption peak in Sr-doped samples can be attributed to the higher reactivity and increased abundance of chemically adsorbed oxygen species, which are closely associated with the formation of oxygen vacancies resulting from the La^{3+} substitution by Sr^{2+}.

The $La_{0.7}Sr_{0.3}CoO_{3-\delta}$ variant exhibits an almost twofold increase in the concentration of O_A species in comparison to $LaCoO_{3-\delta}$. However, at higher lanthanum substitution degrees, there is a reduction in the amount of OA species due to the progressive formation of segregations. These segregations diminish the specific surface area and mask the oxygen vacancies on the surface [40]. In summary, it can be inferred that $La_{0.7}Sr_{0.3}CoO_{3-\delta}$ possesses a higher number of oxygen vacancies, leading to enhanced oxygen adsorption and activation capabilities.

Fig. 4 shows the X-ray Photoelectron Spectroscopy (XPS) characterization, to ascertain the chemical states of the elements on the surface and understand the impact of Sr-doping on $LaCoO_{3-\delta}$. All binding energies were referenced to the C 1s peak at 284.8 eV. Lower oxidation states of cobalt (Co) have the potential to enhance the redox properties. In the presence of reactive oxygen, Co undergoes partial oxidation, and the oxidized Co species subsequently get re-oxidized by oxygen in the gas phase [41]. The unstable oxidation states of Co^{3+} and Co^{2+} are recognized as significant contributors to the catalytic activity of $La_{1-x}Sr_xCoO_{3-\delta}$ [42].

The surface atomic ratios of Co^{2+}/Co^{3+} and O_A/O_L for $La_{1-x}Sr_xCoO_{3-\delta}$ perovskites were determined by calculating the deconvoluted peak areas. The Co^{2+}/Co^{3+} molar ratio exhibited an increase from 11.66 % in $LaCoO_{3-\delta}$ to 21.31 % in $La_{0.7}Sr_{0.3}CoO_{3-\delta}$, suggesting that Sr doping led to the transformation of some Co^{3+} into Co^{2+}. Subsequently, the Co^{2+}/Co^{3+} ratio reached its maximum value for $La_{1-x}Sr_xCoO_{3-\delta}$ and gradually decreased. This phenomenon is linked to the reduction in the specific surface area and the oxygen vacancies at the surface due to phase segregation [40]. In summary, a correlation was observed between the Co^{2+}/Co^{3+} ratio and the Sr^{2+} content. Greater Sr content on the catalyst surface resulted in the generation of a higher proportion of Co^{2+} species [43,44], leading to the formation of structural defects and augmenting the catalyst's oxidation capacity [24,45].

The O1s spectra were deconvoluted into two distinct peaks, as shown in Fig. 4b, signifying the presence of two distinct oxygen species on the catalyst surface. The peaks located at 531.3 and 528.5 eV were ascribed to adsorbed oxygen (OA) and lattice oxygen (OL), respectively. Notably, OA actively participates in oxidation reactions, and a higher concentration of OA on the perovskite surface enhances its oxidation capabilities [46].

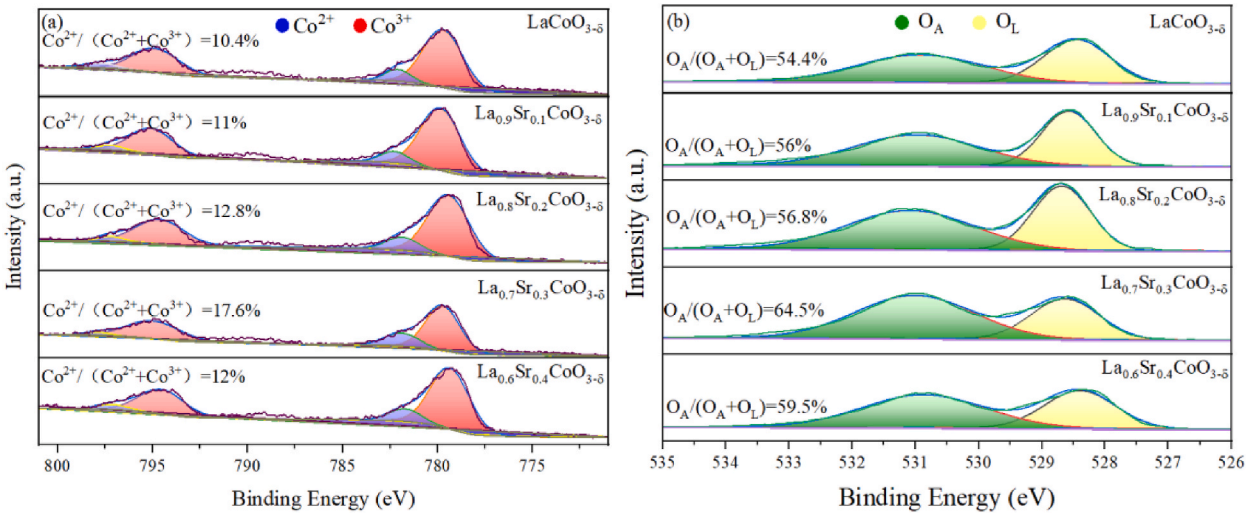

Fig. 4. XPS spectra of Co 2p (a) and O 1s (b) for $La_{1-x}Sr_xCoO_{3-\delta}$(x = 0,0.1,0.2,0.3,0.4).

Furthermore, the density of OA/(OA + OL) can be employed to reflect the quantity of oxygen vacancies [20,46]. Experimental results reveal that the intensity of OA/(OA + OL) increases with the growing Sr concentration, indicating that Sr doping facilitates the generation of oxygen vacancies. However, when the Sr doping reaches 0.4, the amount of adsorbed oxygen on the surface decreases. This could be attributed to the excessive accumulation of $SrCO_3$ on the surface when the Sr doping level becomes too high (x > 0.3). This accumulation covers the surface and occludes some interstitial pores, leading to a reduction in the specific surface area of the samples. Consequently, the decrease in the surface area diminishes the number of oxygen vacancies and oxygen species on the sample surface [24], aligning with the conclusions drawn from XRD and H_2-TPR results.

In perovskite oxide materials, the replacement of high-valence ions at the A-site with lower-valence ions necessitates charge compensation to maintain electrical neutrality. Currently, two approaches are commonly employed to achieve charge compensation in perovskite oxides: adjusting the valence state of B-site ions and increasing the concentration of oxygen vacancies [47].

Given that the oxidation state of Sr ions is lower than that of La ions, when Sr ions substitute La ions, it increases the oxidation state of Co ions or the creation of oxygen vacancies [48]. This is particularly evident in the $La_{0.7}Sr_{0.3}CoO_{3-\delta}$ sample, which exhibits the highest $Co^{2+}/(Co^{2+}+Co^{3+})$ and OA/(OA + OL) molar ratios. The results indicate that as Sr doping occurs, the sample primarily compensates for charge through the generation of oxygen vacancies and Sr incorporation promotes the formation of oxygen vacancies, providing adsorption sites for oxygen molecules. The increase in oxygen vacancies enhances the activation of oxygen and improves the catalytic performance of perovskite oxides [49].

3.2. NO-to-NO_2 oxidation catalyst activity of $La_{1-x}Sr_xCoO_{3-\delta}$

To investigate the impact of $La_{1-x}Sr_xCoO_{3-\delta}$ (x = 0, 0.1, 0.2, 0.3, 0.4) on the NO oxidation performance, the NO conversion ratios of these catalysts over a temperature range of 150–450 °C were determined, shown in Fig. 5. All the samples exhibit a similar trend in NO oxidation capacity with varying temperatures. At lower temperatures, the NO conversion remains minimal, indicating a limitation in NO oxidation at these lower temperature ranges. The conversion of NO to NO_2 on $La_{1-x}Sr_xCoO_{3-\delta}$ gradually increases as the reaction temperature rises and reaches its maximum NO oxidation conversion at 300 °C. Subsequently, the NO conversion decreases, primarily due to thermodynamic constraints associated with the exothermic nature of the reaction [1].

The NO oxidation performances exhibited a descending order as follows: $La_{0.7}Sr_{0.3}CoO_{3-\delta}$ > $La_{0.8}Sr_{0.2}CoO_{3-\delta}$ > $La_{0.6}Sr_{0.4}CoO_{3-\delta}$ > $La_{0.9}Sr_{0.1}CoO_{3-\delta}$ > $LaCoO_{3-\delta}$. Sr-doped samples demonstrated higher conversion rates compared to the non-substituted sample, particularly at intermediate temperatures. When the Sr doping level was below 0.3, the catalytic activity of the catalyst increased with the increasing Sr doping amount. However, when the Sr doping level exceeded 0.3, a decline in the catalyst's activity was observed. Among the prepared samples, $La_{0.7}Sr_{0.3}CoO_{3-\delta}$ perovskites exhibited the most impressive NO-to-NO_2 performance, achieving a maximum conversion of 84 % at 300 °C. This underscores that Sr doping has the potential to enhance the catalyst's oxidation capacity and improve the efficiency of NO oxidation. Within a specific range, the oxidizing ability of the catalyst increases with the rise in the doping level.

The comparison of catalytic oxidation performance of different materials for NO is listed in Table 1. It is found that $La_{0.7}Sr_{0.3}CoO_{3-\delta}$ has better catalytic oxidation performance for NO especially under low temperature and has the potential to replace precious metal catalysts.

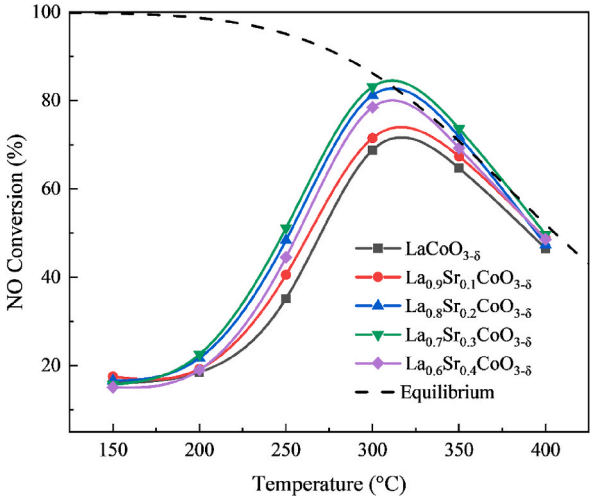

Fig. 5. Catalytic activity of NO conversion of the $La_{1-x}Sr_xCoO_{3-\delta}$ (x = 0,0.1,0.2,0.3,0.4) (inlet gas: 500 ppm NO, 5 % O_2, 5 % H_2O, N_2 balance; GHSV = 200,000 h^{-1}).

Table 1
The Comparison of catalytic oxidation of NO by different materials.

Catalyst	Temperature (°C)	NO conversion	Reference
WO_3	220	92 %	[50]
MoO_3	220	81 %	[50]
Ce–Zr–La modified Pt/γ-Al_2O_3 TWCs	300	14%–17 %	[51]
	400	45%–80 %	[51]
Co_3O_4 NPs	263	93 %	[52]
$SmMn_2O_5$/CNTs	275	85 %	[53]
$SmMn_2O_5$/GO	275	85 %	[53]
$La_{0.7}Sr_{0.3}CoO_{3-\delta}$	300	84 %	This work

3.3. Effect of reaction conditions on catalyst activity

This study investigated the influence of varying airspace and NO and O_2 concentrations on the catalytic oxidation of NO. The research findings have demonstrated that the concentration of NO significantly impacts the catalytic oxidation of NO. Specifically, under conditions characterized by an O_2 concentration of 5 %, NO concentrations ranging from 400 to 800 ppm, and temperatures within the range of 200–300 °C, it was observed that the NO oxidation rate exhibited a declining trend with increasing NO concentration, as depicted in Fig. 6. This phenomenon can be attributed to the fact that, at lower NO concentrations, an ample number of active sites are available on the catalyst's surface. These active sites can promptly adsorb NO and activate O_2, thereby facilitating the catalytic oxidation of NO. As the concentration of NO increased, the active sites on the catalyst surface became increasingly occupied by adsorbed NO molecules, thereby inhibiting the adsorption and activation of O_2. Consequently, the number of reactive oxygen species decreased, leading to a reduced capacity for NO oxidation. Furthermore, when the NO concentration increased from 500 ppm to 700 ppm, the decline in the NO conversion rate was gradual. This suggests that the catalyst demonstrates better adaptability to changes in NO concentration. It is assumed that at high NO concentrations, a portion of the NO may undergo conversion via HNO_x or nitrosyl intermediates present on the catalyst surface. This conversion process could mitigate the influence of NO adsorption on the catalytic oxidation, contributing to the observed adaptability of the catalyst to varying NO concentrations.

Fig. 7 illustrates the impact of airspeed on the catalytic performance of $La_{0.7}Sr_{0.3}CoO_{3-\delta}$ in NO oxidation under specific conditions: an inlet concentration of NO at 500 ppm, an O_2 concentration of 5 %, N_2 as the equilibrium gas, and a temperature range from 250 to 300 °C. The figure reveals a decrease in the NO conversion rate as the airspeed increases from $8 \times 10^4\ h^{-1}$ to $2 \times 10^5\ h^{-1}$. This can be attributed to the fact that at lower airspeeds, NO has ample opportunity for exposure to the catalyst's surface, allowing sufficient time for diffusion into the micropores and completion of the reaction. However, as the airspeed increases, some NO molecules do not have enough time to reach the catalyst's micropores, leading to a decrease in the NO conversion rate. Fig. 7 demonstrates that $La_{0.7}Sr_{0.3}CoO_{3-\delta}$ exhibits good performance within this airspeed range, indicating its adaptability to changes in airspeed.

Fig. 8 shows the influence of O_2 concentration on the rate of NO's catalytic oxidation on $La_{0.7}Sr_{0.3}CoO_{3-\delta}$ under conditions of 200–300 °C, an airspeed of 12000 h^{-1}, and a NO concentration of 500 ppm. With a constant temperature, the conversion rate of NO escalates as the O_2 concentration increases. At lower temperatures, the impact of O_2 on the conversion rate of NO is minimal, potentially due to the low activation of active sites. If these active sites remain inactivated, the rate of conversion from adsorbed oxygen to active oxygen remains slow, even if the adsorbed oxygen has reached saturation. Consequently, the efficiency of NO's

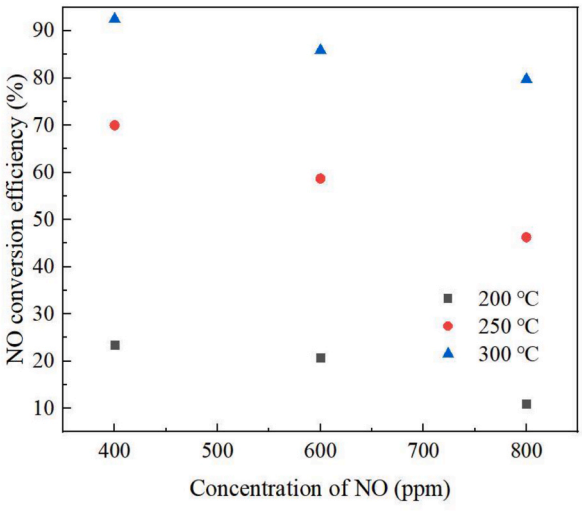

Fig. 6. The effect of concentration of NO on the reaction rate of NO on $La_{0.7}Sr_{0.3}CoO_{3-\delta}$.

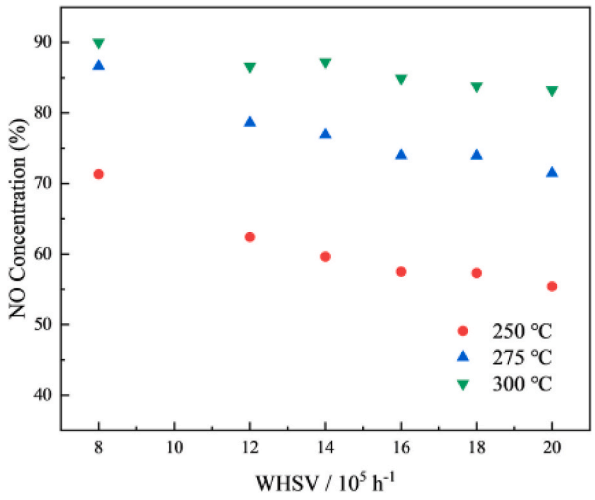

Fig. 7. The effect of airspace on the catalytic oxidation reaction rate of NO on $La_{0.7}Sr_{0.3}CoO_{3-\delta}$.

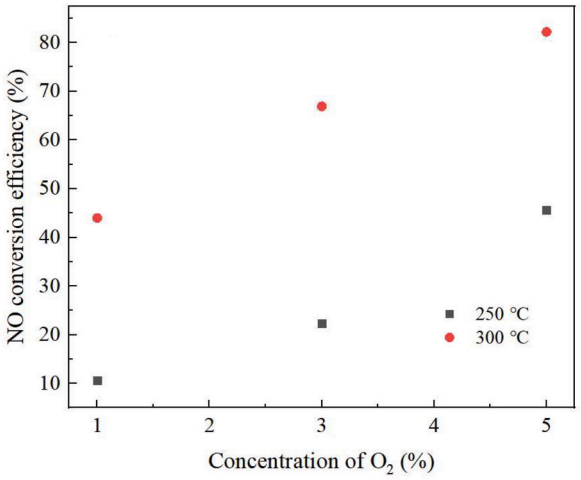

Fig. 8. The effect of O_2 concentration on the catalytic oxidation reaction rate of NO on $La_{0.7}Sr_{0.3}CoO_{3-\delta}$ at different temperatures.

catalytic oxidation only slightly changes with an increase in O_2 content. As the temperature rises, the catalyst's active sites become activated. The O_2 adsorbed at the active site rapidly transforms into activated O_2 and the rate of NO's catalytic oxidation increases with the rising O_2 content. At higher temperatures, the performance of the catalyst for NO oxidation improves as the concentration of oxygen increases. This improvement is primarily attributed to the increased O_2 content, which aids in maintaining reaction equilibrium and enhancing the oxidation rate of NO.

3.4. Reaction path of catalytic oxidation NO–NO_2 on $La_{0.7}Sr_{0.3}CoO_{3-\delta}$ based on kinetic analysis

In kinetic experiments, the integral reactor method was employed to compute reaction rates within a fixed bed. The Eley-Rideal (E-R) and Langmuir-Hinshelwood (L-H) theories were predominantly utilized to explore the mechanisms of catalytic reactions for gas species [54,55]. Consequently, three typical gas-solid catalytic models were established [56]: Model 1. E-R mechanism with O_2 adsorbed (NO free); Model 2. L-H mechanism with both NO and O_2 adsorbed on the same site; Model 3. L-H mechanism with NO and O_2 adsorbed on separate sites. The methods of calculation and the determination of parameters for these models are detailed in the supplementary materials. Experiments were conducted under conditions where the catalyst dosage was 0.1 g and the gas flow rates were 266.67 mL/min, 300 mL/min, and 333.33 mL/min.

Based on the correlation coefficient ® value, it appears that the reaction rate model provides an excellent fit to the experimental results when n equals 0.94. The results of the kinetic parameter calculations are presented in Equation (2).

$$r = 1.55 \times 10^4 \times e^{(-32194.9/RT)} \times C_{NO}^{0.95} \times C_{o_2}^{0.72} \quad (2)$$

The parameters for the three typical gas-solid catalytic models are calculated using the NO conversion rate and are presented in Table 2. R factors are all about 0.999 for all the models, indicating that all models well fit the experimental data. The adsorption of NO and O_2 in different models at various temperatures is detailed in Table 3. The adsorption of O_2 on $La_{0.7}Sr_{0.3}CoO_{3-\delta}$ is stronger than that of NO, and the NO adsorption is significantly less than 1. This indicates that the coverage of NO on the catalyst surface is minimal. These results contradict the assumptions of the E-R and L-H mechanisms regarding NO adsorption. Therefore, the rate-limiting step of the catalytic oxidation reaction of NO on the catalyst surface is the reaction of NO with O_2 adsorbed on the catalyst surface. Consequently, the O_2-adsorbed E-R model may provide a more accurate description of the catalytic oxidation of NO with O_2 on $La_{0.7}Sr_{0.3}CoO_{3-\delta}$.

According to the results of kinetic studies and characterization of $La_{1-x}Sr_xCoO_{3-\delta}$, we assume that the reaction path of catalytic oxidation of NO on $La_{0.7}Sr_{0.3}CoO_{3-\delta}$ as follows:

$$O_2(g) + * \rightarrow *O_2$$

$$*O_2 + * \rightarrow 2*O$$

$$NO + *O \rightarrow NO_2(g) + *$$

Combination reaction:$2NO(g) + O_2 = 2NO_2(g)$

In this process, * is the surface defect site, *O2 is the oxygen molecule adsorbed on an isolated active defect site, *O is the oxygen atom adsorbed on the active defect site, and * NO is the NO adsorbed on the active defect site. The high oxygen adsorption capacity and lattice oxygen mobility are due to the oxygen vacancy produced by Sr doping. This discovery can provide a theoretical foundation for improving the efficiency of NO catalytic oxidation and for subsequent research.

4. Conclusions

In this work, a series of perovskite catalysts, $La_{1-x}Sr_xCoO_{3-\delta}$ ($x = 0, 0.3, 0.4, 0.5, 0.6$) were produced by the sol-gel method. The catalytic performance and reaction pathway of the catalyst for NO oxidation were measured. The results show that Sr-doped perovskite exhibits superior catalytic oxidation activity for NO. The catalytic oxidation performance initially increases and then decreases with the increase in the Sr doping amount. $La_{1-x}Sr_xCoO_{3-\delta}$ ($x = 0.3$) demonstrates the highest NO catalytic oxidation activity, which results from the introduction of Sr. More Sr in the catalyst generates lattice defects, weakens the vibration intensity of La–Co–O bonds, enhances surface oxygen migration, and improves the redox performance of the catalyst, as well as enhances the catalyst's ability to adsorb and store NOx. Moreover, the incorporation of Sr increases the number of oxygen vacancies, which is beneficial for the adsorption and activation of oxygen. As a result, lattice oxygen species are more likely to migrate to the catalyst surface, where they can react with adsorbed NO. However, an excessive introduction of Sr can lead to the formation of $SrCO_3$ heterophases, resulting in some active sites being covered by heterophases, which is not conducive to the catalytic oxidation reaction. The kinetic research results prove that the reaction process of $La_{0.7}Sr_{0.3}CoO_{3-\delta}$ catalytic oxidation NO conforms to the E-R model. The rate-limiting step in the reaction of $La_{0.7}Sr_{0.3}CoO_{3-\delta}$ catalytic oxidation NO is the process of adsorbing O_2 and NO. The surface oxygen space for $La_{0.7}Sr_{0.3}CoO_{3-\delta}$ may be the primary factor affecting NO oxidation efficiency.

Funding

This work was supported by the National Natural Science Foundation of China fig. 52100199]; the China Postdoctoral Science Foundation [2022MD723823].

CRediT authorship contribution statement

Yige Guo: Writing – review & editing, Writing – original draft, Funding acquisition, Formal analysis, Data curation. **Xiaoxue Niu:** Formal analysis, Data curation. **Huaiyu Yang:** Writing – review & editing. **Liwen Chen:** Writing – review & editing. **Yizhen Ren:** Writing – review & editing. **Huining Guo:** Software. **Bo Wu:** Writing – review & editing, Software, Investigation, Formal analysis.

Table 2
The kinetic parameters of different models.

	K	K_1	K_2	R[a]
Model 1	$64667.34 \times exp\left(-\frac{32.02 \times 10^3}{RT}\right)$	$187.61 \times \left(-\frac{386.01}{RT}\right)$	$16.04 \times \left(-\frac{337.36}{RT}\right)$	0.999
Model 2	$2467.02 \times exp\left(-\frac{31.69 \times 10^3}{RT}\right)$	$66.59 \times exp\left(-\frac{372.86}{RT}\right)$	$5.86 \times \left(-\frac{278.01}{RT}\right)$	0.999
Model 3	$615.31 \times \left(-\frac{31.52 \times 10^3}{RT}\right)$	$114.00 \times \left(-\frac{527.24}{RT}\right)$	$14.07\left(-\frac{302 \times 55}{RT}\right)$	0.999

[a] : R is the correlation coefficient.

Table 3
The adsorption of NO and O_2 in different models at various temperatures.

T	P_{NO}	P_{O_2}	Model 1		Model 2		Model 3	
			K_1C_{NO}	$K_2\ C_{O_2}$	K_1C_{NO}	$K_2\ C_{O_2}$	K_1C_{NO}	$K_2\ C_{O_2}$
473.15	40.53	5066.25	0.0680	0.7362	0.024	0.273	0.040	0.651
523.15	40.53	5066.25	0.0687	0.7423	0.024	0.275	0.040	0.656
573.15	40.53	5066.25	0.0692	0.7473	0.025	0.277	0.041	0.660

Declaration of competing interest

The authors declare the following financial interests/personal relationships which may be considered as potential competing interests:Yige guo reports financial support was provided by National Natural Science Foundation of China. Yige guo reports financial support was provided by China Postdoctoral Science Foundation. Yige guo reports financial support was provided by China Scholarship Council. If there are other authors, they declare that they have no known competing financial interests or personal relationships that could have appeared to influence the work reported in this paper.

Appendix A. Supplementary data

Supplementary data to this article can be found online at https://doi.org/10.1016/j.heliyon.2024.e33580.

References

[1] Y. Xin, L. Cheng, Y.N. Lv, J.X. Jia, D.X. Han, N.N. Zhang, J. Wang, Z.L. Zhang, X.M. Cao, Experimental and theoretical insight into the facet-dependent mechanisms of NO oxidation catalyzed by structurally diverse Mn2O3 nanocrystals, Catal 12 (2021) 397–410, https://doi.org/10.1021/acscatal.1c04357.
[2] L. Ma, W. Zhang, Y.G. Wang, X.Y. Chen, W.T. Yu, K. Sun, H.P. Sun, J.H. Li, J.W. Schwank, Catalytic performance and reaction mechanism of NO oxidation over Co3O4 catalysts, Appl. Catal., B 267 (2020) 118371, https://doi.org/10.1016/j.apcatb.2019.118371.
[3] C. Liu, J.W. Shi, C. Gao, et al., Manganese oxide-based catalysts for low-temperature selective catalytic reduction of NOx with NH3: a review, Appl. Catal. Gen. 522 (2016) 54–69, https://doi.org/10.1016/j.apcata.2016.04.023.
[4] Y.D. Chen, X.X. Guan, S.H. Tang, et al., A novel diesel oxidation catalyst with low SO_2 oxidation activity and capable of meeting EuroV emission standards, Chin. J. Catal. 34 (2013) 667–673, https://doi.org/10.1016/S1872-2067(12)60545-2.
[5] X.W. Wang, T. Chen, Y.L. Zhang, et al., Catalytic oxidation of NO over SmMn2O5 nanostructures derived from different Mn precursors, Mol. Catal. 516 (2021) 111983, https://doi.org/10.1016/j.mcat.2021.111983.
[6] S. Adapa, V. Gaur, N. Verma, Catalytic oxidation of NO by activated carbon fiber (ACF), Chem. Eng. J. 116 (1) (2006) 25–37, https://doi.org/10.1016/j.egypro.2019.01.285.
[7] C.H. Liu, S. Porter, J.J. Chen, et al., Enhanced low-temperature performance of bimetallic Pd/Pt/SiO_2(core)@Zr(shell) diesel oxidation catalysts, Appl. Catal. B Environ. 327 (2023) 122436, https://doi.org/10.1016/j.apcatb.2023.122436.
[8] B. Gao, N. Zhang, H.W. Zhang, et al., Effects of platinum high-temperature redispersion on Pt/Al2O3 diesel oxidation catalyst for nitric oxide oxidation and its reaction athway, J. Environ. Chem. Eng. 10 (6) (2022) 108669, https://doi.org/10.1016/j.jece.2022.108669.
[9] J. Suntivich, K.J. May, H.A. Gasteiger, J.B. Goodenough, Y. Shao-Horn, A perovskite oxide Optimized for oxygen evolution catalysis from molecular orbital principles, Science 334 (2011) 1383–1385, https://doi.org/10.1126/science.1212858.
[10] F. Calle-Vallejo, O.A. Diaz-Morales, M.J. Kolb, M.T.M. Koper, Why is bulk thermochemistry a good descriptor for the electrocatalytic activity of transition metal oxides? ACS Catal. 5 (2015) 869–873, https://doi.org/10.1021/cs5016657.
[11] I.C. Man, H.Y. Su, F. Calle-Vallejo, H.A. Hansen, J.I. Martinez, N.G. Inoglu, J. Kitchin, T.F. Jaramillo, J.K. Norskov, J. Rossmeisl, Universality in oxygen evolution electrocatalysis on oxide surfaces, ChemCatChem 3 (2011) 1159–1165.
[12] B. Bza, R.B. Rui, Y.A. Liu, et al., Comparative study of La1–xCexMnO3+δ perovskites and Mn–Ce mixed oxides for NO catalytic oxidation, J. Rare Earths 38 (8) (2020) 863–872.
[13] Q. Gu, L. Wang, Y. Wang, et al., Effect of praseodymium substitution on La1-xPrxMnO3 (x=0–0.4) perovskites and catalytic activity for NO oxidation, J. Phys. Chem. Solid. 133 (2019) 52–58.
[14] R. Zhang, P. Li, L. Ning, et al., Effect of hard-template residues of the nanocasted mesoporous LaFeO3 with extremely high surface areas on catalytic behaviors for methyl chloride oxidation, J. Mater. Chem. A 2 (2014) 17329–17340.
[15] W.F. Libby, Promising catalyst for auto exhaust, Science 171 (3970) (1971) 499–500.
[16] R.J.H. Voorhoeve, J.P. Remeika, D.W. Johnson, Rare earth manganites: catalysts with low ammonia yield in the reduction of nitrogen oxides, Science 180 (4081) (1973) 62–64.
[17] Y.H. Wu, L.L. Li, B.X. Chu, et al., Catalytic reduction of NO by CO over B-site partially substituted $LaM_{0.25}Co_{0.75}O_3$ (M = Cu, Mn, Fe) perovskite oxide catalysts: the correlation between physicochemical properties and catalytic performance, Appl. Catal. Gen. 568 (2018) 43–53.
[18] A. Vazhayil, J. Thomas, N. Thomas, Cobalt doping in LaMnO3 perovskite catalysts-B site optimization by solution combustion for oxygen evolution reaction, J. Electroanal. Chem. 918 (2022) 116426.
[19] L. Dai, X.B. Lu, G.H. Chu, C.H. He, W.C. Zhan, G.J. Zhou, Surface tuning of $LaCoO_3$ perovskite by acid etching to enhance its catalytic performance, Rare Met. 40 (2021) 555–562, https://doi.org/10.1007/s12598-019-01360-w.
[20] L.H. Guo, L. Bo, Y. Li, Z. Jiang, Y. Tian, X. G. L, Sr doping effect on the structure property and NO oxidation performance of dualsite doped perovskite La(Sr)Co(Fe)O_3, Solid State Sci. 113 (2021) 106519, https://doi.org/10.1016/j.solidstatesciences.2020.106519.
[21] N. Alhokbany, A. Sultanah, J. Ahmed, S.I. Al-Saeedi, T. Ahamad, S.M. Alshehri, Investigation of structural and electrical properties of synthesized Sr-doped lanthanum cobaltite ($La_{1-x}Sr_xCoO_3$) perovskite oxide, J. King Saud Univ. Sci. 33 (2021) 101419, https://doi.org/10.1016/j.jksus.2021.101419.
[22] X. Cheng, E. Fabbri, M. Nachtegaal, I.E. Castelli, M.E. Kazzi, R. Haumont, N. Marzari, T.J. Schmidt, Oxygen evolution reaction on $La_{1-x}SrxCoO_3$ perovskites: a combined experimental and theoretical study of their structural, electronic, and electrochemical properties, Chem. Mater. 27 (2015) 7662–7672, https://doi.org/10.1016/j.jksus.2021.101419.
[23] H. Ohbayashi, T. Kudo, T. Gejo, Crystallographic, crystallographic, electric and thermochemical properties of the perovskite-type $ln_{1-x}Sr_xCoO_3$ (Ln: Lanthanoid element), Jpn. J. Appl. Phys. 13 (1974) 1–7, https://doi.org/10.1143/JJAP.13.1.

[24] J.A. Onrubia-Calvo, B.P. Ayo, U.D.L. Torre, J.R. González-Velasco, Key factors in Sr-doped $LaBO_3$ (B = Co or Mn) perovskites for NO oxidation in efficient diesel exhaust purification, Appl. Catal., B 213 (2017) 198–210, https://doi.org/10.1016/j.apcatb.2017.04.068.

[25] S. Rousseau, S. Loridant, P. Delichere, A. Boreave, J.P. Deloume, P. Vernoux, $La_{1-x}Sr_xCo_{1-y}Fe_yO_3$ perovskites prepared by sol–gel method: characterization and relationships with catalytic properties for total oxidation of toluene, Appl. Catal., B 88 (2009) 438–447, https://doi.org/10.1016/j.apcatb.2008.10.022.

[26] S. Ajmal, I. Bibi, F. Majid, S. Ata, K. Kamran, K. Jilani, S. Nouren, Shagufta Kamal, Abid Ali, Munawar Iqbal, Effect of Fe and Bi Doping on $LaCoO_3$ Structural, Magnetic, Electric and Catalytic Properties, vol. 8, 2019, pp. 4831–4842, https://doi.org/10.1016/j.jmrt.2019.08.029.

[27] P. Joshi, M. Saleem, S. Tiwari, J. Shukla, A. Mishra, Diffraction data analysis, microstructure and dielectric studies of transition metal doped $LaCoO_3$, Mate, Proceedings 54 (2022) 890–894, https://doi.org/10.1016/j.matpr.2021.11.206.

[28] P. Jain, S. Srivastava, Investigation of structural, magnetic and electrical properties of pure $LaFeO_3$ synthesized through solution combustion technique, Dig. J. Nanomater. Biostruct. 10 (2015) 141–147.

[29] F. Chao, Q. Gao, G.Y. Xiong, Y.F. Chen, Y. Pan, Z.Y. Fei, Y.P. Li, Y.K. Lu, c. g. Liu, Y.Q. Liu, Defect engineering technique for the fabrication of $LaCoO_3$ perovskite catalyst via urea treatment for total oxidation of propane, Appl. Catal., B 34 (2021) 12100, https://doi.org/10.1016/j.apcatb.2021.121005.

[30] L. Huang, M. Bassir, S. Kaliaguine, Reducibility of Co^{3+} in perovskite-type $LaCoO_3$ and promotion of copper on the reduction of Co^{3+} in perovskite-type oxides, Appl. Surf. Sci. 243 (2005) 360–375, https://doi.org/10.1016/j.apsusc.2004.09.079.

[31] X.W. Wang, T. Chen, Y.L. Zhang, K. Ma, X.R. Wen, C. Sun, Z.H. Yuan, Catalytic oxidation of NO over $SmMn_2O_5$ nanostructures derived from different Mn precursors, Mol. Catal. 516 (2021) 111983, https://doi.org/10.1016/j.mcat.2021.111983.

[32] S. Wang, J.J. Zhu, S.A.C. Carabineiro, P. Xiao, Y.J. Zhu, Selective etching of in-situ formed La_2O_3 particles to prepare porous $LaCoO_3$ perovskite for catalytic combustion of ethyl acetate, Appl. Catal. A-Gen 635 (2022) 118554, https://doi.org/10.1016/j.apcata.2022.118554.

[33] N. Tienthao, M. Hassanzahediniaki, H. Alamdari, S. Kaliaguine, Effect of alkali additives over nanocrystalline Co–Cu-based perovskites as catalysts for higher-alcohol synthesis, J. Catal. 245 (2007) 348–357, https://doi.org/10.1016/j.jcat.2006.10.026.

[34] J.X. Yao, H.Q. Lu, B. Hou, et al., Acidic H_2O_2 treatment of $LaCoO_3$ towards highly dispersed Co3O4 nanoparticles with excellent catalytic performance for C3H8 combustion, Catal. Commun. 135 (2020) 105830.

[35] J.A. Onrubia-Calvo, B. Pereda-Ayo, I. Cabrejas, et al., Ba-doped vs. Sr-doped LaCoO3 perovskites as base catalyst in diesel exhaust purification, Mol. Catal. 488 (2020) 110913.

[36] S. Kośmider, A. Misiewicz, E. Felu, et al., Experimental and clinical studies on the effects of nitrogen oxides on immunity, Int Arch Arbeitsmed 31 (1) (1973) 9–23.

[37] Y.-H. Dong, H. Xian, J.-L. Lv, C. Liu, L. Guo, M. Meng, Y.-S. Tan, N. Tsubaki, X.-G. Li, Influence of synthesis conditions on NO oxidation and NO storage performances of $La_{0.7}Sr_{0.3}MnO_3$ perovskite-type catalyst in lean-burn atmospheres, Mater. Chem. Phys. 143 (2014) 578–586, https://doi.org/10.1016/j.matchemphys.2013.09.035.

[38] H.-J. Eom, J.H. Jang, D.-W. Lee, S. Kim, K.-Y. Lee, Catalytic combustion of hydrogen over $La_{1-x}Sr_xCoO_{3-\delta}$+$Co_3O_4$ and $LaMn_{1-x}Cu_xO_{3+\delta}$ under simulated MCFC anode off-gas conditions, J. Mol. Catal. Chem. 349 (2011) 48–54, https://doi.org/10.1016/j.molcata.2011.08.017.

[39] X. Liu, Y. Guo, Q. He, C. Zhang, Y. Li, Core-shell MnCeO catalysts for NO oxidation and mild temperature diesel soot combustion, J. Rare Earths 41 (4) (2023) 531–538, https://doi.org/10.1016/j.jre.2022.06.012.

[40] A. Mineshige, M. Inaba, T. Yao, et al., Crystal structure and metal–insulator transition of $La_{1-x}Sr_xCoO_3$, J. Solid State Chem. 121 (1996) 423–429.

[41] J. Ding, J. Liu, Y. Yang, Z. Wang, Y. Yu, Reaction mechanism of dichloromethane oxidation on $LaMnO_3$ perovskite, Chemosphere 277 (2021), https://doi.org/10.1016/j.chemosphere.2021.130194.

[42] R. Prasad Neha, S.V. Singh, Simultaneous catalytic oxidation of CO and diesel soot over $LaCoO_3$ perovskite, Mater. Lett. 292 (2021), https://doi.org/10.1016/j.matlet.2021.129588.

[43] C. Díaz, L. Urán, A. Santamaria, Preparation method effect of $La_{0.9}K_{0.1}Co_{0.9}Ni_{0.1}O_3$ perovskite on catalytic soot oxidation, Fuel 295 (2021), https://doi.org/10.1016/j.fuel.2021.120605.

[44] H. Liang, Y. Mou, H. Zhang, S. Li, C. Yao, X. Yu, Sulfur resistance and soot combustion for $La_{0.8}K_{0.2}Co_{1-y}Mn_yO_3$ catalyst, Catal. Today 281 (2017) 477–481, https://doi.org/10.1016/j.cattod.2016.05.015.

[45] D. Zhao, Y. Yang, Z. Gao, Y. Tian, J. Zhang, Z. Jiang, X. Li, A-site defects in $LaSrMnO_3$ perovskite-based catalyst promoting NO storage and reduction for lean-burn exhausts, J. Rare Earths 39 (2021) 959–968, https://doi.org/10.1016/j.jre.2020.04.015.

[46] Q. Wang, L. Ma, L. Wang, D. Wang, Mechanisms for enhanced catalytic performance for NO oxidation over La_2CoMnO_6 double perovskite by A-site or B-site doping: effects of the B-site ionic magnetic moments, Chem. Eng. J. 372 (2019) 728–741, https://doi.org/10.1016/j.cej.2019.04.178.

[47] T. Ishihara, S. Fukui, H. Nishiguchi, et al., Mixed electronic-oxide ionic conductor of BaCoO3 doped with La for cathode of intermediate-temperature-operating solid oxide fuel cell, Solid State Ionics 152 (2002) 609–613.

[48] H. Wang, J. Liu, Z. Zhao, Y. Wei, C. Xu, Comparative study of nanometric Co-, Mn- and Fe-based perovskite-type complex oxide catalysts for the simultaneous elimination of soot and NO_x from diesel engine exhaust, Catal. Today 184 (2012) 288–300, https://doi.org/10.1016/j.cattod.2012.01.005.

[49] J. Yang, S. Hu, Y. Fang, S. Hoang, L. Li, W. Yang, Z. Liang, J. Wu, J. Hu, W. Xiao, C. Pan, Z. Luo, J. Ding, L. Zhang, Y. Guo, Oxygen vacancy promoted O_2 activation over perovskite oxide for low-temperature CO oxidation, ACS Catal. 9 (2019) 9751–9763, https://doi.org/10.1021/acscatal.9b02408.

[50] J. Dawody, M. Skoglundh, E. Fridell, The effect of metal oxide additives (WO3, MoO3, V2O5, Ga2O3) on the oxidation of NO and SO2 over Pt/Al2O3 and Pt/BaO/Al2O3 catalysts, J. Mol. Catal. Chem. 209 (1–2) (2004) 215–225.

[51] A. Papavasiliou, A. Tsetsekou, V. Matsouka, et al., Development of a Ce-Zr-La modified Pt/g-Al2O3 TWCs' washcoat: effect of synthesis procedure on catalytic behavior and thermal durability, Appl. Catal. B Environ. 90 (2009) 162–174.

[52] L. Ma, W. Zhang, Y.G. Wang, et al., Catalytic performance and reaction mechanism of NO oxidation over Co3O4 catalysts, Appl. Catal. B Environ. 267 (2019) 118371.

[53] Tao Chen, Xue-wei Wang, Shi-jing Ma, Xu Ma, Yun-long Zhang, Li-qiu Luo, Zhi-hao Yuan, Carbon nanomaterial-SmMn2O5 nanocrystal composites with highly efficient catalytic oxidation of NO, Solid State Sci. 108 (2020) 106425, https://doi.org/10.1016/j.solidstatesciences.2020.106425.

[54] B. Wu, S.P. Zhang, S.S. He, Y.Q. Xiong, Follow-up mechanism study on NO oxidation with vaporized H2O2 catalyzed by Fe2O3 in a fixed-bed reactor, Chem. Eng. J. 356 (2019) 662–672, https://doi.org/10.1016/j.cej.2018.09.041.

[55] H. Wang, B. Zhang, H. Yang, Q. Bao, B. Wu, New insights on the effects of SO2 on NO oxidation from flue gas with H2O2 vapor over Fe2O3/SiO2, Process Saf. Environ. Prot. 165 (2022) 138–150, https://doi.org/10.1016/j.psep.2022.07.004.

[56] G. Wu, Y. Wang, L. Wang, W. Feng, H. Shi, Y. Lin, T. Zhang, X. Jin, S. Wang, X. Wu, P. Yao, Epoxidation of propylene with H2O2 catalyzed by supported TS-1 catalyst in a fixed-bed reactor: experiments and kinetics, Chem. Eng. J. 215–216 (2013) 306–314, https://doi.org/10.1016/j.cej.2012.11.055.